

## Energy bands and magnetization of a Ni(001) monolayer

Xue-yuan Zhu and J. Hermanson

*Physics Department, Montana State University, Bozeman, Montana 59717*

(Received 16 August 1982)

The calculated energy bands of a Ni(001) monolayer with the bulk lattice parameter display a wide range of exchange splittings influenced by hybridization, potential anisotropy, and bonding differences. The magnetic moment  $0.98\mu_B$  is 75% larger than the measured bulk value of  $0.56\mu_B$ , where  $\mu_B$  is the Bohr magneton. Factors contributing to the increase of magnetization compared with the bulk behavior include narrowing and sharpening of the density of states,  $p$ - $d$  dehybridization, and increased occupation of the  $sp$  band. The majority-spin  $d$  bands are full, in contradiction to previous calculations in which these bands rise above the Fermi energy near  $\bar{M}$  in the surface Brillouin zone. Our results were obtained using a spin-polarized adaptation of the self-consistent localized-orbital method developed by Smith, Gay, and Arlinghaus. We used a new exchange-correlation potential derived from a recent analysis by Vosko, Wilk, and Nusair of the correlation energy of the spin-polarized electron liquid. Substitution of the von Barth-Hedin potential, which overestimates correlation effects, led to a reduction of the magnetic moment by 1%, and a reduction of the exchange splittings by 2–8%.

## I. INTRODUCTION

With the aim of performing accurate theoretical studies of magnetism at  $d$ -band metal surfaces, we have extended the self-consistent local-orbital (SCLO) technique of Smith, Gay, and Arlinghaus<sup>1</sup> to include spin polarization. Our interest in surface magnetism was stimulated by the development of promising new techniques for detecting electron-spin polarization at surfaces, including photoemission,<sup>2–4</sup> tunneling,<sup>5</sup> and field-emission<sup>6</sup> spectroscopies, scattering of spin-polarized electrons,<sup>7</sup> electron-capture spectroscopy,<sup>8</sup> Hall-effect measurements,<sup>9</sup> and ferromagnetic resonance.<sup>10</sup> Indirect evidence of spin polarization has been reported using angle-resolved photoemission spectroscopy, including exchange splittings<sup>11–13</sup> and magnetic surface states.<sup>14–17</sup> Theoretical studies of surface magnetism have been guided by issues such as the relation between surface and bulk magnetization and the factors that control the magnetic behavior. In parametrized tight-binding calculations for a 35-layer Ni(001) film,<sup>18</sup> for example, spin-polarization data<sup>3</sup> were explained in terms of surface states above the majority-spin  $d$  bands. Other workers found an explanation based on modified bulk bands.<sup>19</sup>

Recently, several new computational methods have been applied to  $d$ -band metal surfaces within the local-density approximation.<sup>20,21</sup> To provide a realistic description of the electronic structure, these methods must give due attention to the spatial local-

ization of the  $d$  electrons as well as the expansion of the  $sp$  electron into the vacuum. The potential must be accurately computed from the electron density, and the local-density equations must be iterated to self-consistency. Among the methods devised to treat magnetic surfaces, several stand out by their partial success in meeting these rigid requirements. Wang and Freeman<sup>22</sup> expand the electronic wave function in a minimal basis of (numerical) atomic orbitals. Each spin density is fitted by a sum of spherical atomic charge densities, and matrix elements of the potential are computed by numerical integration in direct space. The method is not fully self-consistent because it constrains the charge density and hence the potential. In addition, the minimal basis may not provide adequate variational freedom. Nonetheless, results obtained for Cu(001) (Ref. 23) are in good agreement with SCLO calculations<sup>1</sup> with a better potential and basis.

When this method was applied to a nine-layer Ni(001) film<sup>22</sup> using a spin-dependent potential of von Barth and Hedin,<sup>21</sup> the surface magnetic moment was found to be 20% less than that of the central plane. This behavior was due in part to a majority-spin surface state at the  $\bar{M}$  point of the surface Brillouin zone, which lay just above the Fermi energy  $E_F$ . While the calculations confirm the nonexistence of magnetically “dead” layers<sup>5–10,24</sup> on Ni(001), they are contradicted by photoemission experiments<sup>14</sup> which place the  $\bar{M}_3$  level below  $E_F$ .

In a second method<sup>25,26</sup> used to study surface

magnetism, the electronic wave function is expanded in augmented plane waves by analogy with the linear (combination of energy-dependent) augmented plane-wave (LAPW) scheme successfully used in the bulk.<sup>27</sup> Deviations of the potential from the muffin-tin form can be included, and the calculations are iterated to self-consistency. For a slab model of Ni(001), the computed moment<sup>25,26</sup> was slightly larger at the surface than at the film center. The LAPW method was also applied to a monolayer of Ni in registry with a Cu(001) substrate.<sup>26</sup> In this case the magnetic moment of the Ni layer was found to be 40% smaller than the bulk value. This reduction was attributed to (1) an unoccupied  $\bar{M}_3$  surface state and (2) charge transfer from Cu to Ni. For the isolated monolayer, Wang, Freeman, and Krakauer<sup>26</sup> obtained a magnetic moment of  $0.86\mu_B$ , significantly larger than the "bulk" value  $0.62\mu_B$ , where  $\mu_B$  is the Bohr magneton. Precise experimental values for the surface magnetization of Ni(001) or Cu(001)-Ni are not available for comparison.

Finally, a cellular method has been applied to ferromagnetic monolayers by Noffke and Fritsche.<sup>28</sup> The spin density is represented as a sum of atomic charge densities as in the method of Wang and Freeman<sup>22</sup>; however, the potential is spherically averaged inside the atomic spheres, while a planar average is performed in the empty cells above and below the monolayer. Within these constraints the calculations are iterated to self-consistency. Computed magnetic moments<sup>28</sup> are larger for Fe, Co, and Ni(001) monolayers than in the bulk, i.e., they are closer to the atomic limit.

In the next section we describe our spin-polarized adaptation of the SCLO method developed by Smith, Gay, and Arlinghaus.<sup>1</sup> The SCLO method has received ample confirmation for paramagnetic  $d$ -band systems through its impressive achievements to date, including the prediction<sup>29</sup> of an  $\bar{M}_3$  surface state on Cu(001) prior to its observation in angle-resolved photoemission experiments.<sup>30</sup> We also discuss an improved exchange-correlation potential drawn from a careful analysis of electron-liquid correlation energies.<sup>31</sup> The latter potential is compared with the commonly used von Barth—Hedin potential.<sup>21</sup> Our method is tested in Sec. III by applying it to a ferromagnetic Ni monolayer with the bulk lattice parameter. The unsupported monolayer was chosen for its simplicity, as well as its conceptual importance as a bridge between the atomic limit and surface magnetism.

We discuss bandwidths, exchange splittings, densities of states, and the magnetization of the monolayer, and compare them with other published work.<sup>25,26,28</sup> We also report results obtained using the von Barth—Hedin potential,<sup>21</sup> which overesti-

mates correlation effects at high electron density.<sup>31</sup> Both the exchange splittings and the magneton number are decreased slightly by this potential. Some comments on the relation of our results to surface-state bands<sup>14,16</sup> on Ni(001) are also included. Finally, a summary is given in Sec. IV.

## II. METHOD

In the SCLO method<sup>1</sup> the wave function in a repeated-slab geometry is expanded in a basis of atomic orbitals developed in a prior calculation for the free atom. Each orbital is fitted to a linear combination of even-tempered Gaussians<sup>32</sup> so that subsequent integrations can be evaluated in closed form.<sup>33</sup> The minimal basis of occupied atomic orbitals is augmented by a set of virtual orbitals for variational freedom. The starting potential is derived from overlapping atomic charge densities, and potential variations are expanded in a discrete Fourier series.

The only numerical integrations in the SCLO method are those for the Fourier coefficients of *changes* in the valence-charge density and the exchange-correlation potential during iteration, which vary slowly in space. The core-charge density is held fixed in its atomic form. At each iteration of the local-density equations, the Hamiltonian is diagonalized at a set of special points<sup>34</sup> in the surface Brillouin zone; the charge density is obtained by summing the probability density  $|\psi|^2$  over the occupied levels. A convergence factor technique is used to stabilize the approach to self-consistency. The various approximations, such as the basis size and the number of  $\mathbf{k}$  points used to compute the charge density, can be tested and refined at will, as demonstrated in detail for Cu(100) in Ref. 1.

We now outline our spin-polarized version of the SCLO method. Beginning with the converged electronic structure of the paramagnetic slab, we break the spin symmetry by rigidly lowering (raising) the energy levels of the majority- (minority-) spin subsystems; a typical value of the trial spin splitting is 0.5 eV. The new system of levels has a new Fermi energy, determined such that the total number of occupied states below  $E_F$  is 28 per Ni atom. The majority- and minority-spin densities,  $\rho(\uparrow)$  and  $\rho(\downarrow)$ , are computed by summing  $|\psi(\uparrow)|^2$  and  $|\psi(\downarrow)|^2$  over occupied levels at 15 special points in the irreducible surface Brillouin zone. Then the potentials  $V(\uparrow)$  and  $V(\downarrow)$  are computed from the spin densities. While the electrostatic Hartree potential depends on the total charge density, and is the same for both spins, the exchange-correlation potential is spin dependent; it will be discussed below. The Hamiltonian is diagonalized for each spin separately. The output energy levels and wave functions set

the stage for the next iteration. With the use of a convergence factor of 0.01 to 0.1, the procedure is continued until all  $d$ -band matrix elements converge within 50 meV.

We now describe the integration mesh used in the Fourier integrals for the charge density and potentials. For the monolayer calculations the mesh size is 0.124 Å within a distance of 1.24 Å (half the atomic spacing) on either side of the film center, and 0.248 Å outside this region. The charge density decreases to  $10^{-10}$  Å<sup>-3</sup> at a distance of 6.2 Å from the film center, where the integration mesh is terminated. In the repeated-slab geometry used here the unit cell is a rectangular prism with a square base 2.48 Å on a side and a height of 20.59 Å. There are 12 000 mesh points in the unit cell, or 850 inequivalent points. We use the denser mesh to ensure that changes of  $d$ -electron occupancy are described properly. As a figure of merit, the total valence charge ( $\vec{Q}=0$  transform of the charge density) differs from 10 electrons by about 0.1%. For a mesh size of 0.248 Å the discrepancy is as large as 2%. This small departure from charge neutrality is removed by renormalization. As a bonus, the calculations converge more rapidly when the finer mesh is used. Results obtained using a mesh size of 0.248 Å differed by less than 0.01 eV and  $0.01\mu_B$  for monolayer energy levels and the magnetic moment. Earlier calculations<sup>1</sup> showed that a mesh size of 0.24 Å gives accurate energy levels for copper films. A coarse mesh is adequate to describe changes of charge density from the starting (atomic) form because the Coulomb and exchange interactions emphasize the wave-vector region near  $\vec{Q}=0$ .

The number of Fourier coefficients which must be included for an exact fit of the charge density and potentials at all mesh points is prescribed in the discrete Fourier-transform method we use.<sup>1</sup> For a mesh size of 0.124 Å the maximum value of  $Q_x$ ,  $Q_y$ , or  $Q_z$  is 25.34 Å<sup>-1</sup>; this defines a "superzone" containing 67 200 reciprocal-lattice vectors. Fortunately, Fourier coefficients of the Coulomb and exchange-correlation potentials (referenced to the starting potentials) decay rapidly in  $\vec{Q}$  space. These have maxima at or near  $\vec{Q}=0$  and fall off by 2 orders of magnitude half the distance to the superzone boundaries; we retain only those  $\vec{Q}$  vectors that lie inside this distance.

Our exchange-correlation potential was adapted from recent studies of the spin-polarized electron liquid by Vosko, Wilk, and Nusair.<sup>31</sup> These authors noted that the commonly used von Barth-Hedin potential<sup>21</sup> is accurate in the high-density range important in transition metals,  $r_s \sim 1$  ( $r_s$  is the mean interelectronic spacing in atomic units). They used a Padé technique to interpolate accurate results for the

random-phase-approximation correlation energy, valid for small  $r_s$ , to low density, where Monte Carlo results are available.<sup>35</sup> To determine a convenient form of the correlation potential, we first fit the paramagnetic correlation energy<sup>31</sup> as

$$\epsilon_c(r_s, 0) = -AF(r_s/R), \quad (1)$$

where

$$F(x) = (1+x^3) \ln \left[ 1 + \frac{1}{x} \right] + \frac{x}{2} - x^2 - \frac{1}{3},$$

$A$  is 48.6 mRy, and  $R$  is 15. This simple formula fits the correlation energy of Ref. 31 to better than 1 mRy for  $r_s$  in the range 1–10. We also fit the spin stiffness (Ref. 31)  $\alpha_c$  (second derivative of the correlation energy with respect to spin polarization) to Eq. (1) with  $A_\alpha = 31.1$  mRy and  $R_\alpha = 16.4$ ; again the fit was better than 1 mRy. The spin-dependent correlation energy can be written as<sup>31</sup>

$$\epsilon_c(r_s, p) = \epsilon_c(r_s, 0) + \frac{1}{2} \alpha_c(r_s) p^2, \quad (2)$$

provided the spin polarization  $p < 0.2$ . The exchange energy in Rydberg units is<sup>20</sup>

$$\epsilon_x(r_s, p) = -(0.916/r_s) [(1+p)^{4/3} + (1-p)^{4/3}]. \quad (3)$$

Within the local-density approximation,<sup>20,21</sup> the exchange-correlation potential for the inhomogeneous system is determined from Eqs. (1)–(3); we find the result

$$V_{xc}^\pm = V_x^\pm + V_c^\pm, \quad (4)$$

where the exchange potential for majority (+) and minority (–) spin in rydbergs is

$$V_x^\pm = -(1.221/r_s)(1 \pm p)^{1/3}, \quad (5)$$

and the correlation potential is

$$V_c^\pm = -A \ln(1 + R/r_s) \pm \alpha_c p + \beta_c p^2, \quad (6)$$

where

$$\beta_c = \frac{1}{2} A_\alpha \ln \left[ 1 + \frac{R}{r_s} \right] - \alpha_c.$$

The term  $\beta_c p^2$  in Eq. (6) is less than 1 mRy for  $r_s = 1$  and  $p < 0.15$ . Note that Eq. (5) may also be expanded in powers of  $p$ ; the spin stiffness  $\alpha_x$  due to exchange is  $-0.407/r_s$  Ry. The exchange splitting may be estimated as  $2|\alpha_x + \alpha_c|p$ , or about 0.9 eV when  $r_s = 1$  and  $p = 0.10$ .

As shown in Table I, correlation reduces the spin stiffness due to exchange by 20–50% for  $r_s$  in the range 1–5. This illustrates the well-known tendency

TABLE I. Spin stiffness of the homogeneous electron liquid for different values of the density parameter  $r_s$ . The exchange contribution  $\alpha_x$  is reduced in magnitude by the correlation contribution  $\alpha_c$ . The von Barth–Hedin potential predicts the values of  $\alpha_c$  given in the last column.

$r_s$	$\alpha_x$ (mRy)	$\alpha_c$ (mRy)	
		Our fit of Ref. 31	von Barth–Hedin potential (Ref. 21)
0.5	-814.5	99.6	122.7
1.0	-407.3	79.4	94.7
2.0	-203.6	60.2	68.2
3.0	-135.8	49.9	53.7
4.0	-101.8	43.0	44.2
5.0	-81.5	38.0	37.3
6.0	-67.9	34.2	32.0

for correlation to oppose ferromagnetism. The von Barth–Hedin potential overestimates the effect for  $r_s < 5$ ;  $\alpha_c$  is 19% larger than our result at  $r_s = 1$ . Thus exchange splittings and magnetic moments computed with the latter potential may be somewhat too small. A comparison of the paramagnetic potentials is given in Table II. Again, the von Barth–Hedin potential overestimates correlation: At  $r_s = 1$ , the enhancement of exchange is 14%, compared with our value of 11%.

### III. RESULTS

The computed energy bands of a ferromagnetic Ni(001) monolayer, obtained using the potential of Eq. (4) and the bulk lattice parameter, are given in Fig. 1;  $E_F$  is the energy zero. The work function, 4.8 eV, is slightly larger than the value 4.7 eV found for the paramagnetic monolayer<sup>36</sup> using Wigner's interpolation formula for the correlation energy.<sup>37</sup>

TABLE II. Exchange and correlation potentials  $V_x^0$  and  $V_c^0$  of the unpolarized electron liquid for different values of the density parameter  $r_s$ . The von Barth–Hedin correlation potential is given in the last column.

$r_s$	$-V_x^0$ (mRy)	$-V_c^0$ (mRy)	
		Our fit of Ref. 31	von Barth–Hedin potential (Ref. 21)
0.5	2442	166.9	207.2
1.0	1221	134.7	173.1
2.0	610.5	104.0	139.7
3.0	407.0	87.1	120.9
4.0	305.2	75.7	107.9
5.0	244.2	67.4	98.1
6.0	203.5	60.9	90.3
10.0	122.1	44.5	69.9

The Wigner potential is less attractive at small  $r_s$  than Eq. (6) with  $p=0$ . For the ferromagnetic monolayer, a work function of 5.7 eV was reported in Ref. 25.

We choose the  $z$  axis perpendicular to the monolayer, and the  $x$  and  $y$  axes along the bulk [100] and [010] directions. In this system the  $\bar{\Sigma}$  line is parallel to the  $x$  axis and the  $\bar{\Delta}$  line is at  $45^\circ$ , as shown in the inset of Fig. 1. Our symmetry labels conform to the character tables of Ref. 38, although we have added primes to denote representations that are odd under  $z$  reflection (the point group  $D_{4h}$  of the monolayer contains a mirror plane not present in the group  $C_{4v}$  of the surface). The odd bands, derived from  $xz$  and  $yz$   $d$  orbitals, may cross any of the unprimed bands in Fig. 1.

Except for the exchange splittings, the bands of the ferromagnetic monolayer are similar to those of the paramagnetic case.<sup>36,39</sup> The  $d$  bands are 30% narrower than the bulk bands, and the  $s$ -band minimum  $\bar{\Gamma}_{11}$  is only 4.86 eV below  $E_F$ , while the bulk value<sup>40</sup> is 8.91 eV. These results are due to the reduced coordination. The exchange splitting, given in Table III, shows a wide variation, from 0.20 eV ( $\bar{X}_3$ ) to 1.08 eV ( $\bar{\Gamma}_4$ ). The average exchange splitting near  $E_F$  is about 1.0 eV; other workers<sup>26</sup> report the value 0.88 eV. Our results are in good overall agreement with Ref. 25.

TABLE III. Exchange splittings for a Ni(001) monolayer at symmetry points in the surface zone. Symmetry labels conform to the character tables of Ref. 18; primes denote odd symmetry under  $z$  reflection. The dominant orbital character of each level is also given.

Symmetry	Orbital character	Exchange splitting (eV)	
		Potential of Eq. (4)	von Barth–Hedin potential (Ref. 21)
$\bar{\Gamma}_1$	$s$	0.25	0.24
$\bar{\Gamma}_3$	$xy$	0.84	0.80
$\bar{\Gamma}_1$	$3z^2 - r^2$	0.76	0.74
$\bar{\Gamma}_5'$	$(xz, yz)$	1.02	0.95
$\bar{\Gamma}_4$	$x^2 - y^2$	1.08	1.06
$\bar{X}_1$	$xy$	0.75	0.72
$\bar{X}_3$	$(x+y)z$	0.91	0.84
$\bar{X}_2$	$x^2 - y^2$	1.03	1.00
$\bar{X}_1$	$3z^2 - r^2$	0.84	0.82
$\bar{X}_4'$	$(x-y)z$	1.03	0.96
$\bar{X}_3$	$x+y$	0.20	0.19
$\bar{M}_4$	$x^2 - y^2$	0.86	0.84
$\bar{M}_5'$	$(xz, yz)$	0.94	0.88
$\bar{M}_1$	$3z^2 - r^2$	0.91	0.89
$\bar{M}_3$	$xy$	1.02	0.97

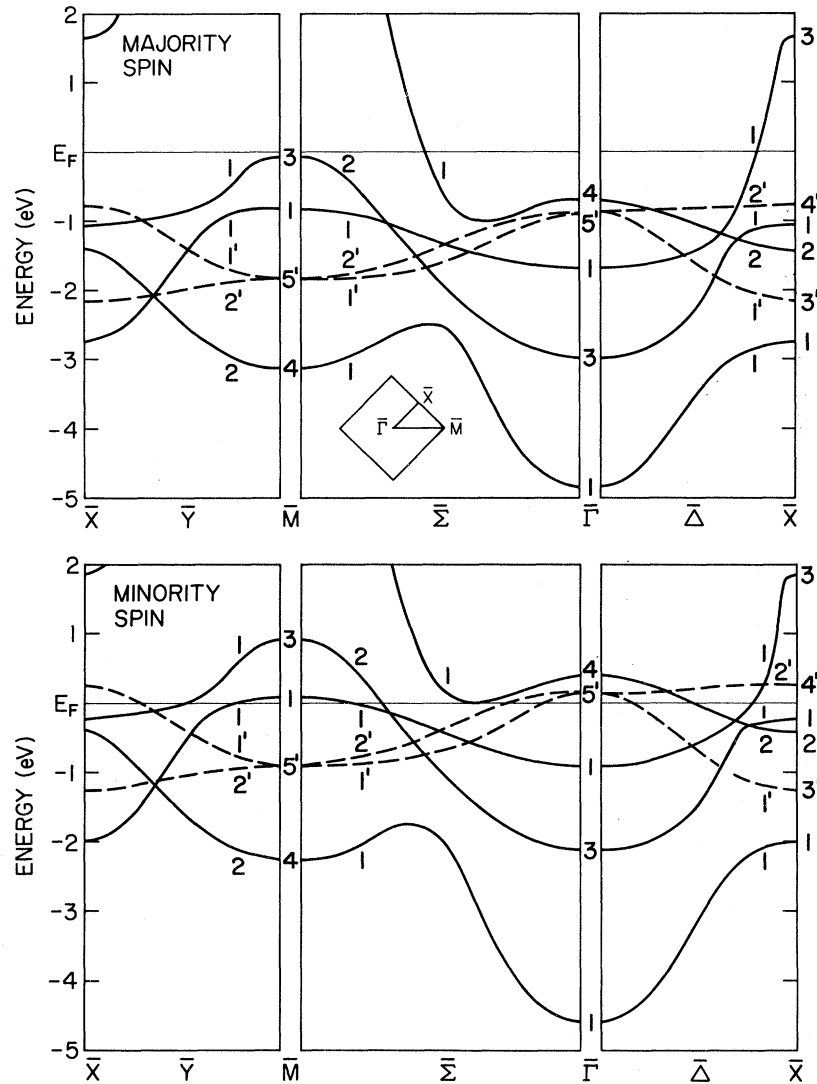


FIG. 1. Spin-polarized energy bands of a Ni(001) monolayer, based on the potential of Eq. (4). The surface Brillouin zone is shown in the inset, using standard labels for the symmetry points and lines (Ref. 38). Symmetry labels agree with Ref. 38; primes denote odd symmetry under  $z$  reflection.  $E_F$  is the energy zone.

Three factors influence the exchange splittings in Fig. 1: (1)  $sp$ - $d$  hybridization, (2) orbital symmetry, and (3)  $\vec{k}$ -dependent bonding differences. The first aspect is illustrated by the  $sp$  bands along  $\bar{\Sigma}$  and  $\bar{\Delta}$ : Their splittings are small except where they overlap the  $d$  bands. The splittings are roughly proportional to the  $d$ -orbital content. Secondly, Table III shows that  $d$ -orbital symmetries play an important role; this effect is associated with the anisotropy of the self-consistent potential and is presumably smaller in calculations which assume spherical symmetry inside the atomic spheres.<sup>26,28</sup> The third factor affecting exchange splittings is the  $\vec{k}$ -dependent phase contained in the Bloch function, which produces bonding differences within a single  $d$  band. For ex-

ample, consider the  $\bar{\Gamma}_3$ - $\bar{M}_3$  band in Fig. 1. The orbital character is  $xy$  ( $t_{2g}$ ), with a small  $p_y$  component along  $\bar{\Sigma}$  (other orbitals are excluded by symmetry). At  $\bar{\Gamma}$ ,  $xy$  orbitals on neighboring atoms overlap constructively, pulling charge away from the atoms to conserve the normalization; thus the exchange splitting 0.84 eV is less than that at  $\bar{M}$ , 1.02 eV, where destructive overlap occurs. Similarly, for the  $e_g$  ( $x^2-y^2$ ) levels  $\bar{\Gamma}_4$  and  $\bar{M}_4$ , the bonding level  $\bar{M}_4$  is split by 0.86 eV, the antibonding level  $\bar{\Gamma}_4$  by 1.08 eV.

The spin-resolved density of states (DOS) for the Ni monolayer was computed using a Monte Carlo sampling technique.<sup>1</sup> The bands computed at 45 special points in the irreducible segment of the Brill-

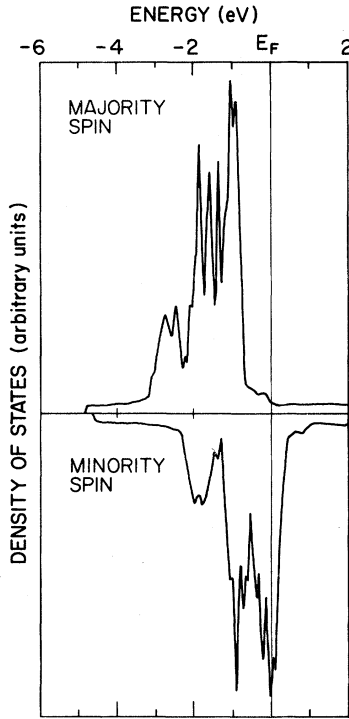


FIG. 2. Spin-resolved densities of states (DOS) for the energy bands of the Ni monolayer.  $E_F$  is the energy zero.

loun zone were interpolated quadratically to  $10^5$  randomly generated points. A histogram generated by counting energy levels that fall in 27-meV-wide channels was smoothed by three-point averaging to eliminate some of the statistical noise. Partial DOS for specific atomic orbitals were obtained by the Mulliken projection technique discussed in Ref. 1, which is appropriate when nonorthogonal basic functions are used. Occupation numbers for each orbital were computed by integrating the partial DOS up to the Fermi energy.

The DOS for majority and minority spin are displayed in Fig. 2. While the minority-spin DOS with its three main peaks, each about 1 eV in width, is similar to the DOS of the paramagnetic monolayer,<sup>36</sup> the majority-spin DOS is rather different. Both DOS have a low steplike threshold due to the  $s$ -band minimum  $\bar{\Gamma}_1$  and a weak shoulder at the  $d$ -band maximum  $\bar{M}_3$  near  $E_F$ . A low-energy doublet structure due to  $\bar{\Gamma}_3$ ,  $\bar{M}_4$ ,  $\bar{X}_1$ , and  $\bar{\Sigma}_1$  critical points is

well separated from more pronounced structures closer to  $E_F$ . The latter contain contributions from the relatively flat  $xz, yz$  bands  $\bar{\Gamma}'_5$ - $\bar{M}'_5$ - $\bar{X}'_3$  and  $\bar{\Gamma}'_5$ - $\bar{X}'_4$ , as well as the critical points  $\bar{\Gamma}_4$ ,  $\bar{\Gamma}_1$ ,  $\bar{X}_1$ ,  $\bar{M}_1$ , and  $\bar{\Sigma}_1$ . The failure of the spin-resolved DOS to replicate each other is due to the variable exchange splittings noted above.

Contributions of each valence orbital to the magnetic moment  $\mu$  and the valence charge  $z$  are given in Table IV. Note that the converged configuration  $d^{8.73}s^{0.98}p^{0.29}$  differs from the starting configuration  $d^9s^1$ , mainly by the transfer of about 0.3 electrons into  $p$  orbitals due to hybridization. The variations of  $\mu$  and  $z$  among the  $d$  levels are due to (1) the position of  $E_F$  within the minority-spin bands (see Fig. 1) and (2) hybridization, which reduces the  $d$ -orbital content below  $E_F$ . The narrowest  $d$  band,  $\bar{X}_1$ - $\bar{M}_1$ - $\bar{\Gamma}_1$ - $\bar{X}_1$ , has mainly  $3z^2-r^2$  character, and rises above  $E_F$  only near  $\bar{M}$  for minority spin. Thus the  $3z^2-r^2$  orbital has the largest occupation among the  $d$  levels, 1.86 electrons or 0.14 holes; these contribute only  $0.09\mu_B$  to  $\mu$ . The broadest bands, of primarily  $x^2-y^2$  and  $xy$  character, have the largest extent above  $E_F$ , and contribute 1.69 and 1.70 electrons to the valence charge and  $0.23\mu_B$  and  $0.15\mu_B$  to the magnetic moment, respectively. The  $xz, yz$  orbitals have the largest spin moments,  $0.25\mu_B$  each, due to the flat minority-spin band  $\bar{\Gamma}_5$ - $\bar{X}_4$ , above  $E_F$ .

The unequal  $d$ -level populations give rise to potential anisotropies. The Hartree potential, like the charge density, is nearly cylindrically symmetric in the atomic spheres, since the  $d$  orbitals excluding  $3z^2-r^2$  have nearly equal populations, about 1.7 electrons. On the other hand, the spin density is largest in the  $x$ - $z$  and  $y$ - $z$  planes, since it is dominated by contributions from the  $x^2-y^2$  and  $xz, yz$  orbitals. The resulting anisotropy of the exchange potential *difference*.  $V(\uparrow) - V(\downarrow)$  explains why the latter orbitals tend to have the largest exchange splittings.

We find that the magnetization density changes sign in the interstitial and vacuum regions. This is due to the deeper potential for majority-spin electrons, which pulls them closer to the nuclei. Core polarization could not be studied since the core charge was frozen in its atomic form.

The calculated magnetic moment,  $0.98\mu_B$ , is larger than that obtained by earlier workers, and

TABLE IV. Atomic-orbital contributions to the valence charge  $z$  and magnetic moment  $\mu$ , obtained by integrating the partial DOS for each spin and orbital type.

	$s$	$p$	$d$	$3z^2-r^2$	$x^2-y^2$	$xy$	$xz$ or $yz$
$z$ (electrons)	0.98	0.29	8.73	1.86	1.69	1.70	1.74
$\mu$ ( $\mu_B$ )	0.01	0.00	0.97	0.09	0.23	0.15	0.25

75% larger than the measured bulk value<sup>41</sup> of  $0.56\mu_B$ . Two of the earlier results (Refs. 26 and 28),  $0.86\mu_B$  and  $0.90\mu_B$  (Ref. 26 uses the Cu lattice parameter, which is 2.5% larger than that of Ni), were derived using a spherically symmetrized potential inside the atomic spheres and the von Barth—Hedin treatment of correlation.<sup>21</sup> The third result (Ref. 25),  $0.95\mu_B$ , was based on an anisotropic potential but also used the von Barth—Hedin approximation. We recalculated the monolayer bands using the correlation potential of Ref. 21; the results for exchange splittings are given in Table III. We find, as expected, that the splittings are smaller than we obtained using Eq. (4). The reduction varies from 2% to 8%. The majority-spin  $d$ -band width ( $\bar{M}_{3\uparrow}$ - $\bar{M}_{4\uparrow}$ ) is 3.06 eV in both calculations, and the  $sp$ -band minimum  $\bar{\Gamma}_{1\uparrow}$  is also almost unchanged, at 4.85 eV below  $E_F$ . The magnetic moment is reduced by only 1% to  $0.97\mu_B$ , and is in excellent agreement with Ref. 25.

Several factors increase the monolayer magnetization compared with the bulk. These include band narrowing and dehybridization. Band narrowing is particularly important for the  $\bar{\Gamma}'_5$ - $\bar{X}'_4$  [ $(x-y)z$ ] and  $\bar{M}_1$  ( $3z^2-r^2$ ) minority-spin bands in Fig. 1, since these bands are largely responsible for the DOS peak just above  $E_F$  in Fig. 2. They are narrow because their wave functions are directed towards missing bulk atoms. Similarly, the upper majority-spin band edge, excluding the weak  $\bar{M}_{3\uparrow}$  shoulder, is rather steep. These features of the DOS favor saturation of the  $d$ -band magnetization.

The monolayer  $d$  bands experience less hybridization with  $sp$  bands than in the bulk; this also leads to an increase of the magnetization by strengthening the effective exchange interaction. Earlier workers<sup>28</sup> found that  $p$ -state occupation decreases by 0.43 electrons in the monolayer compared with the bulk, while the  $s$ -state occupation increases by only 0.13 electrons. Their monolayer configuration,  $d^{8.74}s^{0.83}p^{0.43}$ , is in reasonable agreement with our result,  $d^{8.73}s^{0.98}p^{0.29}$ .

The effects discussed above bring the monolayer magnetization closer to the atomic limit. At the Ni(001) surface, the effects will be somewhat diminished by the presence of neighboring atomic layers. Then the magnetic behavior should be intermediate between the monolayer and bulk limits.

An interesting feature of our results is that the majority-spin  $d$  bands are full: The  $d$ -band maximum  $\bar{M}_{3\uparrow}$  is below  $E_F$ . This behavior is also found in the bulk<sup>40</sup> and in the free atom, and is consistent with Hund's rule. Thus the magnetic moment is given by the number of holes in the minority-spin  $d$  band, and is larger in the monolayer because the narrowed  $sp$  band holds more electrons than in the

bulk. Photoemission results for Ni(001) surfaces<sup>14</sup> indicate the  $\bar{M}_{3\uparrow}$  surface state is also occupied. Thus Hund's rule may be universal for the  $d$  bands of nickel, independent of the atomic coordination. Previous theoretical results for (Refs. 22 and 25) Ni(001) violate Hund's rule. For the monolayer, we find that the  $\bar{M}_{3\uparrow}$  level drops below  $E_F$  as the calculations proceed towards self-consistency.

Our computed monolayer bands are closely related to magnetic surface states<sup>14,16</sup> observed on single crystal Ni(001) near  $\bar{\Gamma}$ ,  $\bar{M}$ , and  $\bar{X}$ . Symmetry arguments<sup>42</sup> imply that only  $\bar{\Gamma}_5$  and  $\bar{\Gamma}_1$  surface states contribute to the photocurrent collected along the sample normal.<sup>16</sup> Since the incident light in Ref. 16 was predominantly  $s$  polarized, the weak feature observed near  $E_F$  is presumably a  $\bar{\Gamma}'_5$  ( $xz, yz$ ) state, drawn from the bulk  $\Delta_5$  bands.<sup>42</sup> This state, which was obtained in previous slab calculations,<sup>18,22,25</sup> corresponds to our  $\bar{\Gamma}'_5$  state in Fig. 1. The  $\bar{\Gamma}_4$  level is forbidden by the selection rules.<sup>42</sup> Considerable discussion<sup>18,19</sup> has focused on the question whether the  $\bar{\Gamma}_5$  surface state explains electron spin-polarization data.<sup>3</sup>

The surface-state band observed for mirror-plane emission<sup>14</sup> near  $\bar{M}$  has been attributed to a majority-spin band with odd reflection parity in the (100) plane. It may be described as a Tamm state of  $xy$  character, pushed out of the extremely flat bulk  $Z_2$  band by the surface potential.<sup>30</sup> Because its planar character implies weak overlap with near-surface layers, the Tamm state is practically identical to our monolayer band passing through  $\bar{M}_{3\uparrow}$  in Fig. 1. Slab calculations,<sup>18,22,25</sup> as mentioned above, place the maximum of this band above  $E_F$ , where it could not contribute to the photocurrent observed in Ref. 14.

The even minority-spin surface band<sup>14</sup> observed near  $\bar{X}$  is compatible with our  $\bar{X}_1$  ( $3z^2-r^2$ ) state near  $E_F$ , and the  $\bar{X}'_3$  [ $(x-y)z$ ] and  $\bar{X}_1$  ( $xy$ ) levels at lower energy. An even band has been obtained in the slab calculations<sup>18,22,25</sup> along  $\bar{\Delta}$ , although it lies about 1.5 eV below  $E_F$  in the calculations of Ref. 25, and disperses too rapidly away from  $\bar{X}$  in the other results.<sup>18,22</sup>

The computed monolayer bands will be modified when thicker slabs are considered. While the  $\bar{M}_3$  ( $xy$ ) state has weak interaction with near-surface layers, the  $\bar{\Gamma}$  and  $\bar{X}$  states discussed above may be changed significantly. Note that the  $\bar{\Gamma}'_5$  state will not change its  $d$ -orbital character ( $xz, yz$ ) due to symmetry constraints, nor will the  $\bar{X}'_3$ , but the  $\bar{X}_1$  states of  $3z^2-r^2$  and  $xy$  character may be strongly hybridized. Surface layer magnetization and exchange splittings are expected to be less than the monolayer values but greater than the bulk values.

## IV. SUMMARY

The computed energy bands of the ferromagnetic Ni(001) monolayer show a wide range of exchange splittings, from 0.20 eV at  $\bar{X}_3$  to 1.08 eV at  $\bar{\Gamma}_4$  with an average of about 1.0 eV near  $E_F$ . Hybridization, anisotropy of the self-consistent potential, and  $k$ -dependent bonding differences influence these splittings. Other workers report<sup>26</sup> a value of 0.88 eV near  $E_F$ , but do not discuss its range of variation. Our results are in good overall agreement with earlier calculations<sup>25</sup> based on the LAPW method.

The magnetic moment  $0.98\mu_B$  is somewhat larger than values obtained before<sup>26,28</sup> using spherically symmetrized potentials inside the atomic spheres and the von Barth—Hedin correlation potential, but close to that of Ref. 25,  $0.95\mu_B$ . We find that the  $d$ -band maximum  $\bar{M}_{31}$  for majority spins drops below  $E_F$  as the calculations proceed towards self-consistency; the placement of this level affects the magnetic moment. When the calculations were repeated using the von Barth—Hedin potential in place of Eq. (4), the exchange splittings and magnetization were reduced slightly since correlation is overestimated.<sup>31</sup>

The reduced coordination of Ni atoms in the

monolayer geometry produces several effects which increase the magnetization compared with the bulk behavior. These effects include narrowing and sharpening of the DOS,  $p$ - $d$  dehybridization, and increased occupation of the  $sp$  band. Thus the monolayer is closer to the atomic limit; the magnetic behavior of the surface layer of Ni(001) is expected to be intermediate between the monolayer and bulk limits.

## ACKNOWLEDGMENTS

We are indebted to Dr. J. R. Smith, Dr. J. G. Gay, and Dr. F. J. Arlinghaus of General Motors Research Laboratories for introducing us to their SCLO programs, and for invaluable assistance and discussions during all phases of this work. The expert assistance of the Montana State University Computer Services staff is gratefully acknowledged. We profited from helpful discussions with Professor H. Bross, Sektion Physik der Universität München and Dr. Roy Richter of General Motors Research Laboratories. This work was supported in part by the National Science Foundation MONTS-NSF project No. ISP-80-11449 at Montana State University, Bozeman, Montana.

- <sup>1</sup>J. R. Smith, J. G. Gay, and F. J. Arlinghaus, *Phys. Rev. B* **21**, 2201 (1980).
- <sup>2</sup>U. Baenninger, G. Busch, M. Campagna, and H. C. Siegmann, *Phys. Rev. Lett.* **25**, 585 (1970); D. T. Pierce and H. C. Siegmann, *Phys. Rev. B* **9**, 4035 (1974).
- <sup>3</sup>W. Eib and S. F. Alvarado, *Phys. Rev. Lett.* **37**, 444 (1976).
- <sup>4</sup>E. Kisker, W. Gudat, E. Kuhlmann, R. Clauberg, and M. Campagna, *Phys. Rev. Lett.* **45**, 2053 (1980).
- <sup>5</sup>P. M. Tedrow and R. Meservey, *Phys. Rev. B* **7**, 318 (1973).
- <sup>6</sup>H. C. Siegmann, *Phys. Rev. B* **17**, 37 (1975); M. Landolt and M. Campagna, *Phys. Rev. Lett.* **38**, 663 (1977).
- <sup>7</sup>R. J. Celotta, D. T. Pierce, G.-C. Wang, S. D. Bader, and G. P. Felcher, *Phys. Rev. Lett.* **43**, 728 (1979).
- <sup>8</sup>C. Rau, *Comments Solid State Phys.* **9**, 177 (1980); C. Rau and S. Eichner, *Phys. Rev. Lett.* **47**, 939 (1981).
- <sup>9</sup>G. Bergmann, *Phys. Rev. Lett.* **41**, 264 (1978).
- <sup>10</sup>W. Goepel, *Surf. Sci.* **85**, 400 (1979).
- <sup>11</sup>E. Dietz, U. Gerhardt, and C. J. Maetz, *Phys. Rev. Lett.* **40**, 892 (1978).
- <sup>12</sup>D. E. Eastman, F. J. Himpsel, and J. A. Knapp, *Phys. Rev. Lett.* **40**, 1514 (1978); F. J. Himpsel, J. A. Knapp, and D. E. Eastman, *Phys. Rev. B* **19**, 2919 (1979); D. E. Eastman, F. J. Himpsel, and J. A. Knapp, *Phys. Rev. Lett.* **44**, 95 (1980).
- <sup>13</sup>P. Heimann and H. Neddermeyer, *J. Magn. Magn. Mater.* **15-18**, 1143, (1980).
- <sup>14</sup>E. W. Plummer and W. Eberhardt, *Phys. Rev. B* **20**, 1444 (1979).
- <sup>15</sup>W. Eberhardt, E. W. Plummer, K. Horn, and J. Erskine, *Phys. Rev. Lett.* **45**, 273 (1980).
- <sup>16</sup>J. L. Erskine, *Phys. Rev. Lett.* **45**, 1446 (1980).
- <sup>17</sup>L. Gonzales, R. Miranda, M. Salmeron, J. A. Verges, and F. Yndurain, *Phys. Rev. B* **24**, 3245 (1981).
- <sup>18</sup>D. G. Dempsey and L. Kleinman, *Phys. Rev. Lett.* **39**, 1297 (1977); D. G. Dempsey, W. R. Grise, and L. Kleinman, *Phys. Rev. B* **18**, 1270 (1978).
- <sup>19</sup>I. D. Moore and J. B. Pendry, *J. Phys. C* **11**, 4615 (1978).
- <sup>20</sup>W. Kohn and L. J. Sham, *Phys. Rev.* **140**, A1133 (1965).
- <sup>21</sup>U. von Barth and L. Hedin, *J. Phys. C* **5**, 1629 (1972).
- <sup>22</sup>C. S. Wang and A. J. Freeman, *J. Appl. Phys.* **50**, 1940 (1979); *Phys. Rev. B* **21**, 4585 (1980).
- <sup>23</sup>C. S. Wang and A. J. Freeman, *Phys. Rev. B* **18**, 1714 (1978).
- <sup>24</sup>L. N. Lieberman, J. Clinton, D. M. Edwards, and J. Mathon, *Phys. Rev. Lett.* **25**, 232 (1970).
- <sup>25</sup>O. Jepsen, J. Madsen, and O. K. Andersen, *J. Magn. Magn. Mater.* **15-18**, 867 (1980); *Phys. Rev. B* **26**, 2790 (1982).
- <sup>26</sup>D. S. Wang, A. J. Freeman, and H. Krakauer, *Phys. Rev. B* **24**, 1126 (1981); A. J. Freeman, D. S. Wang, and H. Krakauer, *J. Appl. Phys.* **53**, 1997 (1982).
- <sup>27</sup>D. D. Koelling and G. O. Arbman, *J. Phys. F* **5**, 2041 (1975); O. K. Andersen, *Phys. Rev. B* **12**, 3060 (1975).
- <sup>28</sup>J. Noffke and L. Fritsche, *J. Phys. C* **14**, 89 (1981).

- <sup>29</sup>J. G. Gay, J. R. Smith, and F. J. Arlinghaus, *Phys. Rev. Lett.* **42**, 332 (1979).
- <sup>30</sup>P. Heimann, J. Hermanson, H. Miosga, and H. Neddermeyer, *Phys. Rev. Lett.* **42**, 1782 (1979); *Phys. Rev. B* **20**, 3059 (1979).
- <sup>31</sup>S. H. Vosko, L. Wilk, and M. Nusair, *Can. J. Phys.* **58**, 1200 (1980).
- <sup>32</sup>R. C. Bardo and K. Ruedenberg, *J. Chem. Phys.* **59**, 5956 (1973).
- <sup>33</sup>E. E. Lafon and C. C. Lin, *Phys. Rev.* **152**, 579 (1966); J. Langlinais and J. Callaway, *Phys. Rev. B* **5**, 124 (1972).
- <sup>34</sup>S. J. Cunningham, *Phys. Rev. B* **10**, 4988 (1974).
- <sup>35</sup>D. M. Ceperly, *Phys. Rev. B* **18**, 3126 (1978).
- <sup>36</sup>F. J. Arlinghaus, J. G. Gay, and J. R. Smith, *Phys. Rev. B* **21**, 2055 (1980).
- <sup>37</sup>E. P. Wigner, *Phys. Rev.* **46**, 1002 (1934); *Trans. Faraday Soc.* **34**, 678 (1938); D. Pines, *Elementary Excitation in Solids* (Benjamin, New York, 1963), p. 91.
- <sup>38</sup>G. P. Alldredge and L. Kleinman, *Phys. Rev. B* **10**, 559 (1974).
- <sup>39</sup>C. S. Wang and A. J. Freeman, *Phys. Rev. B* **19**, 793 (1979).
- <sup>40</sup>C. S. Wang and J. Callaway, *Phys. Rev.* **15**, 298 (1977).
- <sup>41</sup>H. Danan, R. Heer, and A. J. P. Meyer, *J. Appl. Phys.* **39**, 669 (1968). The measured magnetic moment  $0.616\mu_B$  contains an orbital part which must be subtracted to give the spin magnetic moment  $0.56\mu_B$ ; see C. Kittel, *Introduction to Solid State Physics*, 5th ed. (Wiley, New York, 1976), p. 466.
- <sup>42</sup>J. Hermanson, *Solid State Commun.* **22**, 9 (1977).